Two-Body Interatomic Potentials for He, Ne, Ar, Kr and Xe from *Ab Initio* Data

U. K. Deiters

Institut für Physikalische Chemie, University of Cologne, Luxemburger Str. 116, D-50939 Köln, Germany

Richard J. Sadus[a]

Centre for Computational Innovations, Swinburne University of Technology, PO Box 218, Hawthorn, Victoria 3122, Australia

Abstract

A new method is reported for developing accurate two-body interatomic potentials from existing *ab initio* data. The method avoids the computational complexity of alternative methods without sacrificing accuracy. Two-body potentials are developed for He, Ne, Ar, Kr and Xe, which accurately reproduce the potential energy at all inter-atomic separations. Monte Carlo simulations of the pressure, radial distribution function and isochoric heat capacity using the simplified potential indicate that the results are in very close, and sometimes almost indistinguishable, agreement with more complicated current state-of-the-art two-body potentials.

---

[a] Author for correspondence, email: rsadus@swin.edu.au.

I. INTRODUCTION

The macroscopic properties of materials, irrespective of whether in the liquid, gas or solid state, are ultimately determined by the nature of interactions between their constituent atoms or molecules.[1] In most instances, the dominant contribution from such interatomic or intermolecular interactions can be attributed to the sum of interactions between all of the different pairs of atoms or molecules, i.e. two-body interactions. Although it is well-documented[2-4] that the addition of three– or more-body interactions are required for an accurate representation of the properties of materials, the dominance of two-body interactions means that understanding such interactions is of paramount importance.

Information regarding two-body interactions is accessible via experimental properties such as second virial coefficients or viscosities of dilute gases. From a theoretical perspective, two-body interactions can be evaluated via molecular simulation.[5] Except for 'on-the-fly' simulation techniques such as the Car-Parrinello method,[6] the latter approach requires the postulation of a two-body interatomic or intermolecular potential ($u(r)$) to determine either the energy or force of interaction between the particles at a given separation (r).

The noble gases have been the focus of many investigations[7-25] for two-body potentials. The earliest successful two-body potentials for Ar or Kr adopted a semi-empirical approach involving fitting a potential to two-body experimental data. An example of this approach is the Barker-Fisher-Watts (BFW) potential,[11] which has the following form

$$\frac{u(r)_{BFW}}{\varepsilon} = \sum_{i=0}^{5} A_i \left(R-1\right)^i e^{\alpha(1-R)} - \sum_{n=6,8,10} \frac{C_n}{\delta + R^n},$$

(1)

where $R = r/r_{min}$ and r_{min} defines the interatomic separation at which the potential has a minimum (ε). The potential involves the C_6, C_8 and C_{10} dispersion coefficients; the remaining terms were obtained by

fitting to experimental data. In contrast, more recent advances in computational chemistry[26] have witnessed the development of two-body potentials from first principles or *ab initio* data.[8, 13, 14, 27] The advent powerful quantum mechanical methods—particularly the CCSD(T) method—and the improvement of computers, pair potentials of increasing accuracy have been developed. The reader is referred to refs. 8, 13, 14 and 27 and publications cited therein.

In a series of publications,[16-25] Jäger, Hellmann, Bich and Vogel (JHBV) have reported highly accurate two-body *ab initio* data for all the stable noble gases, which they used to obtain analytical two-body potentials. A modified aug-cc-pV7Z basis set was used[17] for He. Calculations for Ne, Ar and Kr used correlation-consistent basis sets[21,22] involving polarized-valence sextuple-zeta contributions, which was further extended[25] for Xe.

For He, the JHBV potential is based in part on the formula of Tang and Toennies.[28]

$$u(r)_{\text{JHBV}} = A\exp\left(a_1 R + a_2 R^2 + a_{-1}R^{-1} + a_{-2}R^{-2} + d_1\sin(d_2 R + d_3)\right) - \sum_{n=3}^{8} f_{2n}(bR)\frac{C_{2n}}{R^{2n}} \qquad (2)$$

where

$$f_{2n}(x) = 1 - e^{-x}\sum_{k=0}^{2n}\frac{x^k}{k!}. \qquad (3)$$

In Eq. (2), $R = r/\sigma$, which is the interatomic separation relative to the separation (σ) at which $u(r) = 0$. The parameters A, a_1, a_2, a_{-1}, a_{-2}, b, d_1, d_2 and d_3 where fitted to the *ab initio* data with $f_{2n}(x) = 1$. The C_{2n} terms are the dispersion coefficients.

There are some subtle variations for the different atoms but the general form for the JHBV potential for Ne, Ar, Kr and Xe is

$$u(r)_{JHBV} = A\exp\left(a_1 R + a_2 R^2 + a_{-1} R^{-1} + a_{-2} R^{-2}\right) - \sum_{n=3}^{8} f_{2n}(bR)\frac{C_{2n}}{R^{2n}}, \quad R < R_{sr}$$

$$u(r)_{JHBV} = \frac{\tilde{A}}{R}e^{-\tilde{\alpha}R} \qquad\qquad R \geq R_{sr}$$

(4)

where R_{sr} is an atom-specific short range cut-off distance. The second term is used to extend the JHBV potential to interatomic separations not covered by the *ab initio* data. Comparison with Eq. (2) shows that accurately representing the properties of He necessitates an additional term that is not required for the remaining noble gases.

Although the JHBV potentials are highly accurate and arguably 'state-of-the-art,' they are computationally expensive and as such impractical for the evaluation of the properties of materials. The computational difficulty is largely caused by the adoption of the Tang and Toennies[28] formula, which also forms the basis of alternative interatomic potentials such as the Nasrabad and Deiters[8] Patkowski and Szalewicz[15] potentials. The evaluation of the second term of Eq. (4) involves a nested summation involving Eq. (2). This alone imposes a considerable computational cost for the evaluation of energy, which is compounded further when a derivative is required to obtain either the virial or the force. The requirement for a substitute potential at small interatomic separations is also computationally undesirable.

It is not advisable to omit the short-range potential. If neither parameter a_{-1} nor a_{-2} is positive, the uncorrected JBHV potential runs to negative-infinite values for $R \rightarrow 0$. The simulation ensemble of a Monte Carlo simulation using the uncorrected JBHV potential is likely to collapse to a state of infinite density.

The aim of this work was to develop alternative interatomic two-body potentials to accurately represent the *ab initio* data for noble gases at minimal computational cost at all interatomic separations.

A new method for the development of interatomic potentials is reported, which is in principle transferable to other cases. It results in a compact and mathematically simpler interatomic potential.

II.   THEORY

A.   Development of a new two-body potential

The selection of the functional form of the new two-body potential was guided by the following considerations:

1. A proper two-body or pair potential function $u(r)$ intersects the abscissa exactly once at the distance ("collision diameter") σ. It is positive and monotonously decreasing for $r < \sigma$, and it is negative for $r > \sigma$; in the latter range it passes through a single minimum.

2. At long distances, $u(r)$ is dominated by dispersion interactions. Therefore it must monotonously converge against zero according to r^{-6}.

3. At short distances, $u(r)$ is dominated by Pauli repulsion (orbital overlap). As discussed by Pathak and Thakkar[30] as well as by Deiters and Neumaier,[9] this repulsion can be described approximately by an $\exp(r)/r$ term.

4. In particular, $u(r)$ must approach $+\infty$ for $r \rightarrow 0$.

Figure 1 shows the behavior of $u(r)\, r^6$ (energy measured in K) as a function of distance. In accordance with the requirements listed above, this function exhibits a high (positive) maximum at short distances and a shallow (negative) minimum after the only intersection with the abscissa. It runs towards a constant negative value at large distances. The diagram suggests a function containing a constant negative term, plus an exponential term with a small decrement for the attractive well, plus an $\exp(r)/r$ term with a large decrement for the repulsion zone. The resulting simplified *ab initio* atomic potential (SAAP) is

$$u_{\text{SAAP}} = \frac{\left(\dfrac{a_0}{r}\right)\exp(a_1 r) + a_2 \exp(a_3 r) + a_4}{1 + a_5 r^6},$$

(5)

with a_0, $a_5 > 0$ and $a_{1\ldots4} < 0$. Helium, for which *ab initio* data at extremely small distances are available, requires one additional parameter in the repulsive exponential. The extended potential (SAAPx) then becomes

$$u_{\text{SAAPx}}(r) = \frac{\left(\dfrac{a_0}{r}\right)\exp(a_1 r + a_6 r^2) + a_2 \exp(a_3 r) + a_4}{1 + a_5 r^6},$$

(6)

$a_6 < 0$. Evidently, this pair potential can also be used for the other noble gases by setting $a_6 = 0$.
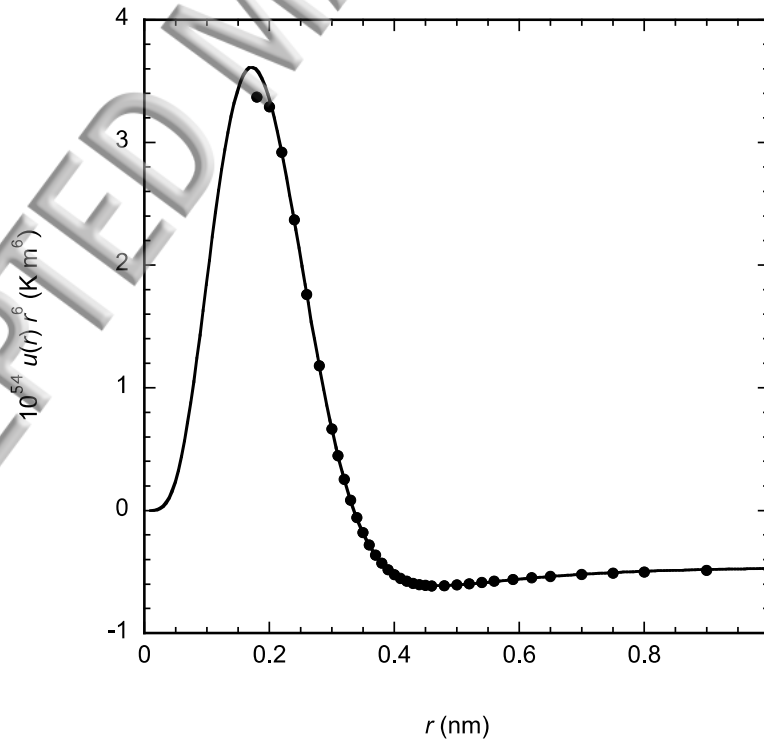
FIG 1. Comparsion of the SAAP behavior for $u(r)\, r^6$ (solid line) with *ab initio* data ($\bullet$) for Ar.

6

The numerical values of the parameters of the various noble gases were determined by fitting $u_{SAAP}(r)$ or u_{SAAPx}, respectively, to the *ab initio* noble gases data of Jäger, Hellmann, Bich and Vogel.[16-25] For argon, neon, and helium a weight function $\exp(-\sigma/r)$ was applied to enforce a better agreement in the regions of thermodynamic relevance.

The parameters for the noble gases are summarised in Table I. Figure 2 illustrates the values of the parameters with respect to the atomic number (Z). In both Table I and Figure 2, the a_i parameters are reduced with respect to ε and σ. It is apparent from Table I that there is relatively little variation in the reduced values of a_1, a_3, a_4 and a_5. In contrast both a_0 (Figure 2) and a_2 (Figure 2) vary greatly with Z, which indicates their importance in capturing the different chemical nature of the atoms. We observe that the magnitudes of a_0 and a_2 parameters (Table I) are not consistent with the overall trend for the other noble gases, which may reflect uncertainties the nature of the parameter estimation as discussed above as well as strong correlations between the parameters.

TABLE I. Summary of the two-body SAAP and SAAPx parameters obtained in this work.

	He (SAAPx)	He	Ne	Ar	Kr	Xe
ε/k (K)	10.92536561	11.00963377	42.36165080	143.4899372	201.0821392	280.1837503
σ (nm)	0.2639244581	0.2639781646	0.2759124561	0.3355134529	0.357999364	0.3901195551
$a_0/\varepsilon\sigma$	24238.01564	81648.44026	211781.8544	65214.64725	60249.13228	44977.3164
$a_1\sigma$	-5.934943188	-9.829947619	-10.89769496	-9.452343340	-9.456080572	-9.121814449
a_2/ε	-11.17928721	-6.482831445	-20.94225988	-19.42488828	-24.40996013	-29.63636182
$a_3\sigma$	-1.821078761	-0.5073208921	-2.317079421	-1.958381959	-2.182279261	-2.278991444
a_4/ε	-0.7762283939	-0.4906026951	-1.854049559	-2.379111084	-1.959180470	-1.876430370
a_5/σ^6	0.3703465767	0.9921472732	0.7454617542	1.051490962	0.874092399	0.8701531593
a_6/σ^2	-3.210773756	0	0	0	0	0
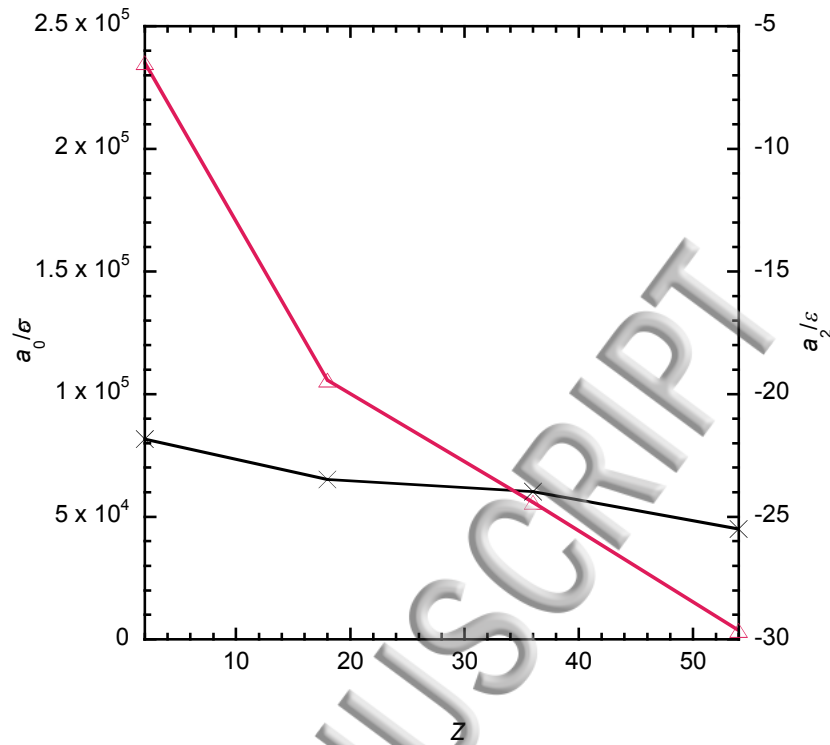
FIG 2. The value of the reduced SAAP a_0 (×) (LHS y-axis) and a_5 (△) (RHS y-axis) parameters as a function of atomic number. The lines through the data are for guidance only.

Compared to the JHBV potential (Eq. (4)), the SAAP has two simple exponential terms, but more importantly, the need for the nested summation terms involving the dispersion coefficients has been eliminated. The SAAP needs only 6 or 7 parameters, whereas 14 parameters are required for Eq. (4). It is also valid at all interatomic separations and as such it does not require an alternative pair potential at small separations.

B. Simulation details

Canonical (*NVT*) Monte Carlo (MC) simulations were performed for which the number of particles (*N*), volume (*V*) and temperature (*T*) were held constant. A system size of 1000 atoms was used and periodic boundary conditions were applied. Initial configurations were created by placing the atoms at random locations in a very large cubic simulation box, and then compressing this to the

desired volume. The cut-off radius was set to 4σ, and corresponding long-range corrections were evaluated numerically using Romberg's method.[30] The simulation ensembles were equilibrated for 40,000 cycles (with a simulation cycle consisting of N attempted particle displacements); after that, statistical data were collected from 800,000 cycles (4 parallel threads of 200,000 cycles). The maximum displacement size was adjusted continually to achieve a 50% acceptance rate. The ensemble pressure was calculated using the virial theorem.[5] The residual isochoric heat capacity (C_{Vr}) was obtained from fluctuations of the total potential energy (U) of the system,[1,5] i.e.,

$$C_{Vr} = \frac{1}{kT^2 N}\left[\left\langle U^2\right\rangle - \left\langle U\right\rangle^2\right],\tag{7}$$

where U is calculated by summing the all the distinct pairs of atoms interacting via the potential, and the angled brackets denote ensemble averages. The structure of the noble gases was investigated by calculating the RDF ($g(r)$) from the standard following formula[1]

$$g(r) = \frac{V}{4\pi\rho^2 N(N-1)}\left\langle \sum_i n_i(r)\Delta r\right\rangle,\tag{8}$$

where $n(r)\Delta r$ is the number of atoms that exist in the region between r and $r+\Delta r$; here a channel width Δr of 0.01 nm was used.

III. RESULTS AND DISCUSSION

A. Potential energy curve for He

As described above in the development of the SAAP, He poses considerable challenges requiring an additional parameter resulting in the SAAPx. The difficulty has also been recognised in

other He potentials. Figure 4 compares *ab initio* data with SAAP and SAAPx calculations in the vicinity of the potential minimum.
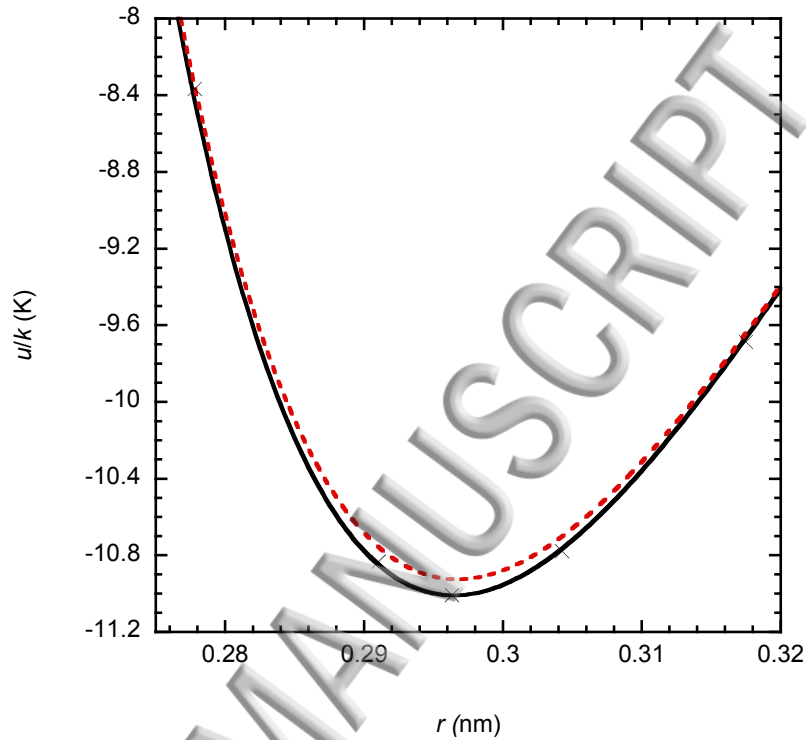
FIG 3. Comparison of the *ab initio* potential energy of He (×) with SAAP (solid line) and SAAPx (dashed line) calculations at interatomic separations close to the attractive well.

Both potentials yield reasonably good agreement with the *ab initio* data, however the SAAPx slightly overestimates the potential energy in the vicinity of potential minimum..
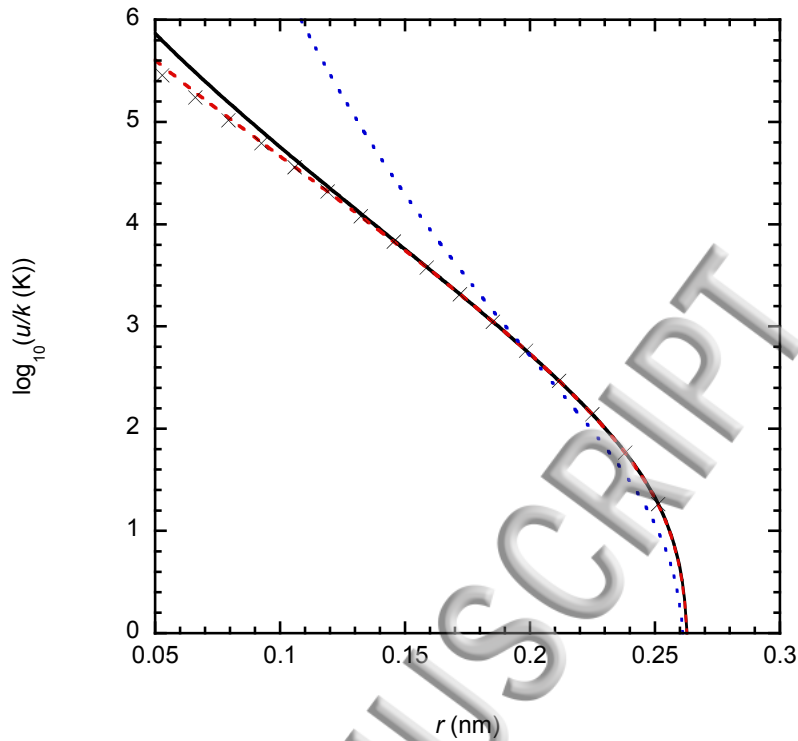
FIG. 4. Comparison of the *ab initio* potential energy of He ($\times$) with SAAP (solid line) and SAAPx (red dashed line) calculations at interatomic separations in the repulsive region. Calculations with the Lennard-Jones potential (blue dashed line, $\varepsilon/k = 6.03$ K, $\sigma = 0.263$ nm) are also included.

Interatomic separations that correspond to dominantly repulsive contributions to the potential energy are illustrated in Figure 4. The SAAP provides an accurate presentation of repulsion until $r \approx$ 0.12 nm where after the SAAPx is required, because otherwise the repulsion would be too steep. Figure 5 also includes a comparison with the 12-6 Mie potential (i.e., the Lennard-Jones potential), which greatly exaggerates repulsion starting from separations of $r \approx 0.12$ nm.

B.   Potential energy curves of Ne, Ar, Kr and Xe

A comparison of the overall potential energy predicted by the SAAP with *ab initio* two-body data is given in Figure 5.
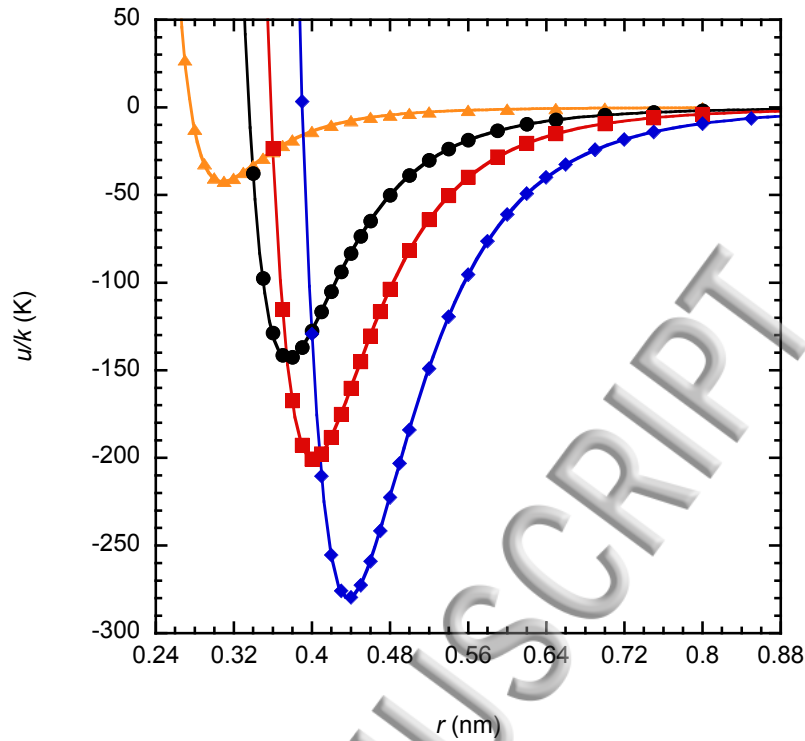
FIG. 5. Comparison of *ab initio* potential energies for Ne (▲), Ar (●), Kr (■) and Xe (◆) with SAAP calculations (solid lines).

It is apparent from Figure 5 that the SAAP predicts the two-body potential energy of the remaining noble gas to a high degree of accuracy. The potential minimum, repulsive region and interactions occurring at large separations are all predicted accurately. This is also the case at small separations (Figure 6), which are often quite challenging to describe accurately. Figure 6 also illustrates a comparison with the Lennard-Jones potential, which starts becoming too repulsive even at modest separations of $r \approx 0.34$ nm and $r \approx 0.38$ nm for Kr and Xe, respectively.
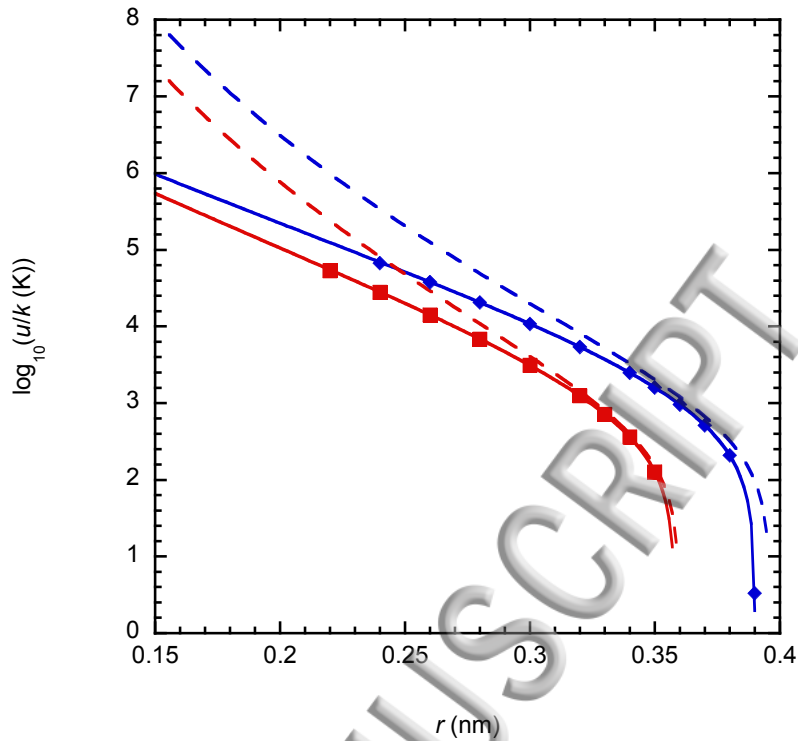
FIG. 6. Comparison of *ab initio* potential energies for Kr (■) and Xe (◆) at repulsive interatomic separations with SAAP calculations (solid lines). Calculations with the Lennard-Jones potential (corresponding dashed lines) for Kr ($\varepsilon/k = 171.0$ K, $\sigma = 0.360$ nm) and Xe ($\varepsilon/k = 217$ K, $\sigma = 0.395$ nm) are also included.

It is apparent from the preceding analysis of the noble gases that the SAAP reproduces the *ab initio* potential energies to a high degree of accuracy. Nonetheless, the limited number of parameters used means that it is unrealistic to exactly match the quality of agreement with the multi-parameter JHBV potential, particularly at small interatomic separations. The question is what effect does the relatively small differences between the SAAP and the JHBV potential have on predicted properties? To address this issue, we analysed predicted RDFs, p and C_{Vr} from molecular simulation.

C.   RDFs

The RDFs of Ar at $T = 130$ K and both $V = 28.5$ cm^3/mol and $V = 500$ cm^3/mol are illustrated in Fig. 7. These state points were chosen because Ar is in the homogeneous liquid and vapor phase, respectively.
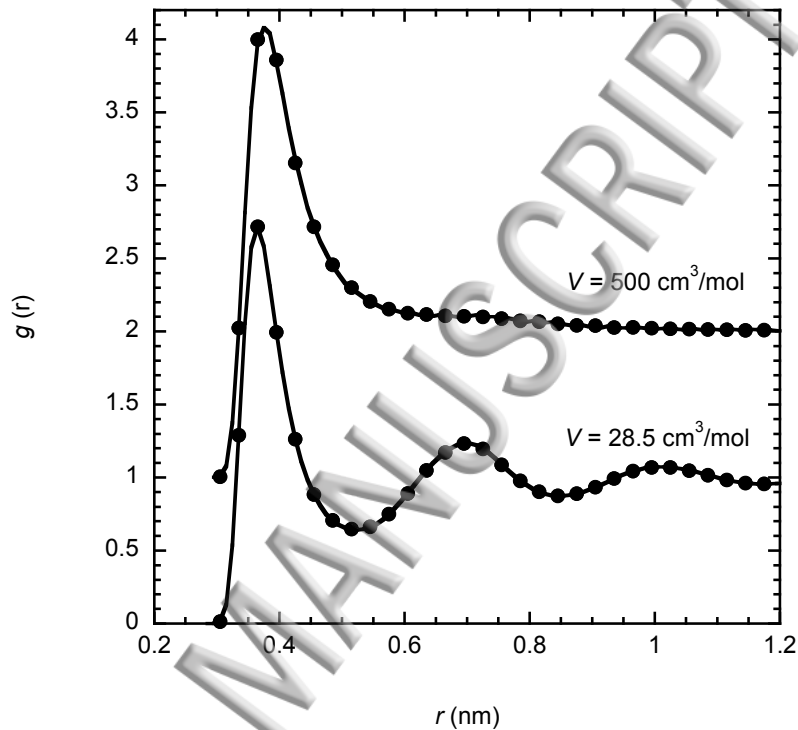
FIG. 7. Comparison of RDFs obtained from the JHBV potential (solid line) for Ar with results obtained for the SAAP (●) in liquid (28. 5 cm^3/mol) and vapor (500 cm^3/mol) phases at $T = 130$ K. The RDFs for the vapor phase are shifted by $+ 1$.

It is apparent from Figure 7 that the results for the SAAP and JHBV potential are almost indistinguishable from each other, indicating that the SAAP potential faithfully reproduces the *ab initio* structure of the fluid in both vapor and liquid phases.

Having established the equivalence between the SAAP and JHBV potential, we compared the predictions of the SAAP with experimental RDFs. Such a comparison for Ar is illustrated in Fig. 8 for experimental data[31,32] of a liquid state (ambient pressure, $T = 85$ K) close to the triple point and a dense

14

supercritical state (p = 87.7 MPa, T = 85 K). It is apparent from Fig. 8 that the SAAP accurately represents the RDFs at both these extreme conditions.
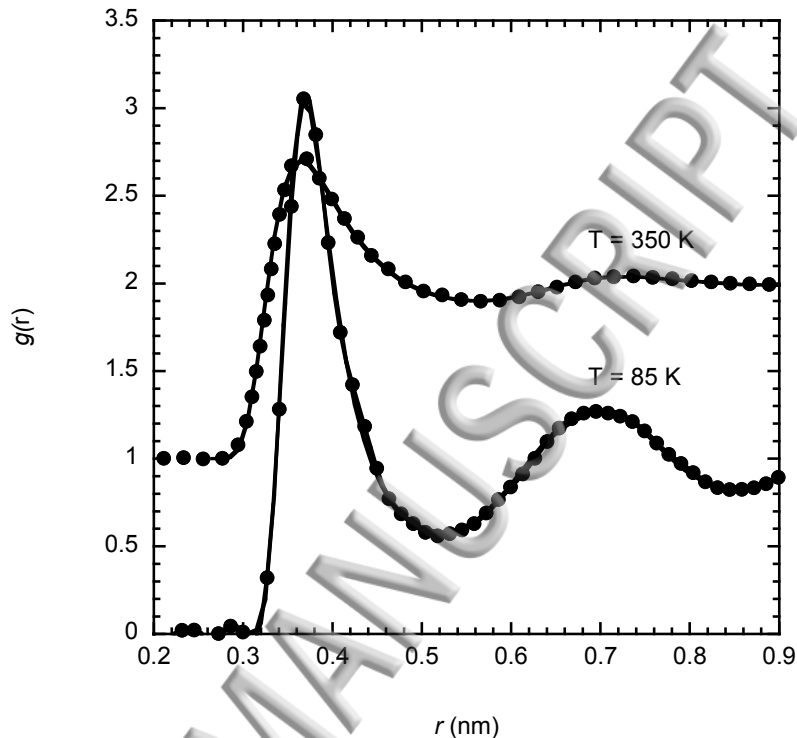
FIG. 8. Comparison of experimental RDF data[31,32] (●) at T = 85 (V = 28.27 cm^3/mol) and 350 K (V = 49 cm^3/mol) with predictions from the SAAP (solid lines). The data for 350 K are shifted by +1.

D. p and C_{Vr}

The values of both p and C_{Vr} predicted for Ar by the JHBV potential and the SAAP are illustrated in Fig. 9. It is apparent from this comparison that C_{Vr} declines with increasing p. The results obtained for p with the SAAP are almost indistinguishable from the JHBV potential values. Good agreement is also observed for C_{Vr}, although the SAAP values are consistently slightly lower than those obtained for the JHBV potential. It should be noted that the SAAP was not fitted to the JHBV potential, but evaluated independently from *ab* initio data. In the absence of *ab initio* p and C_{Vr} data, the relative

accuracy of the two potentials cannot be determined. We note that, as discussed elsewhere,[33] obtaining C_{Vr} values from first principles are both difficult and prone to considerable uncertainties.
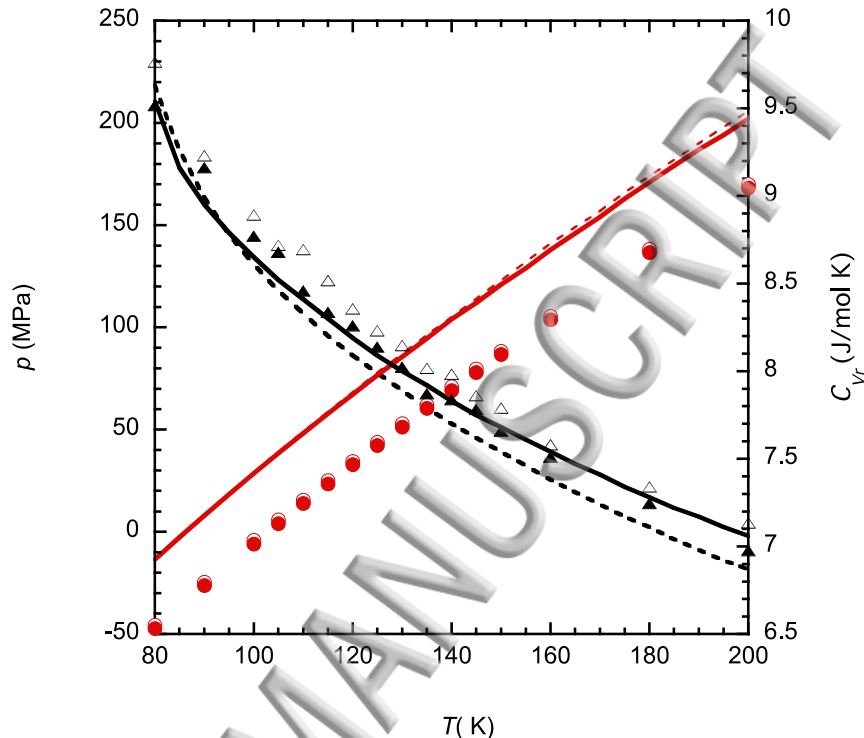
FIG 9. Comparison of p (LHS y-axis) and C_{Vr} (RHS y-axis) for Ar predicted by the JHBV potential ((p(○), C_{Vr} (△)), the SAAP (p(●), C_{Vr} (▲)) and the Lennard-Jones potential (red and black dashed lines) for V = 28.5 cm³/mol. The corresponding experimental values[34] (red and black solid lines) are also illustrated. At most values of T, the JHBV and SAAP results for p almost exactly coincide with each other.

Figure 9 also provides a comparison with both experimental data[34] and calculations with the Lennard-Jones potential. Both the SAAP and JHBV potential under-predict p, which can be expected because they are genuinely two-body potentials, whereas p has well-documented[2,5] contributions from three- or more-body interactions. For reasons that are discussed below, the Lennard-Jones calculations over-predict p at $T > 140$ K. The SAAP and the JHBV potential both yield good agreement with experimental C_{Vr} data, whereas the Lennard-Jones potential under-predicts this property at most temperatures. This suggests that C_{Vr} for Ar is dominated by two-body interactions.

A similar comparison for p and C_{Vr} predicted for the SAAP and JHBV potential and for Xe is given in Fig. 10. In common with Ar, p values obtained for the two potentials are in excellent agreement over the entire temperature range. Comparison with experimental data indicates that the two-body potentials under-predict p. The calculations with the Lennard-Jones potential are in better agreement with experiment but straddle the data either side of 500 K.
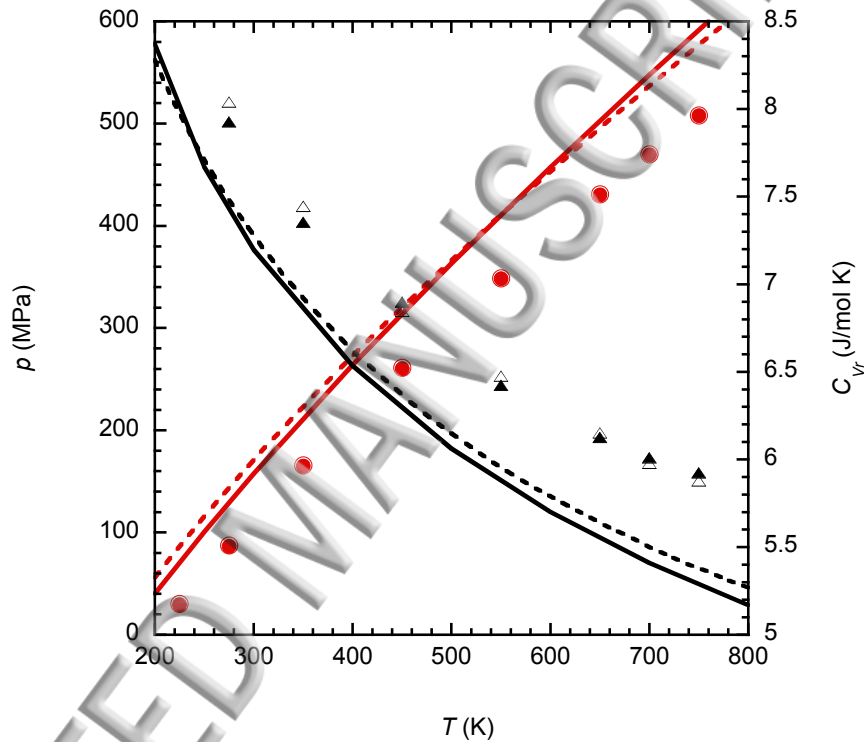
FIG 10. Comparison of p (LHS y-axis) and C_{Vr} (RHS y-axis) for Xe predicted by the JHBV potential (($p(\bigcirc)$, C_{Vr} ($\triangle$)), the SAAP ($p(\bullet)$, C_{Vr} ($\blacktriangle$)) and the Lennard-Jones potential (red and black dashed lines) for $V = 45$ cm^3/mol. The corresponding experimental values[35] (red and black solid lines) are also illustrated. At most values of T, the JHBV and SAAP results for p almost exactly coincide with each other.

The C_{Vr} values for both two-body potentials shown in Fig. 10 are also in close agreement. However, in contrast to the very good agreement at all values of T obtained for Ar, both the SAAP and the JHBV potential predict values of C_{Vr} for Xe that are noticeably higher than the experimental data.[35] Furthermore, unlike the Ar case, the Lennard-Jones calculations do not under-predict C_{Vr}. The

discrepancy with experiment can be at least partly attributed to the greater role of three-body and other multi-body interactions for the considerably larger Xe atom. Calculations for Kr (not illustrated in Fig. 9) also overestimate C_{Vr} but the magnitude of the discrepancy is smaller than for Xe. This is consistent with the contribution of non-additive interatomic interactions being proportional to the atomic weight. It has been previously established[33] that two-body interactions alone are inadequate for the prediction of the thermodynamic properties of either He or Ne, which require accounting for quantum effects.
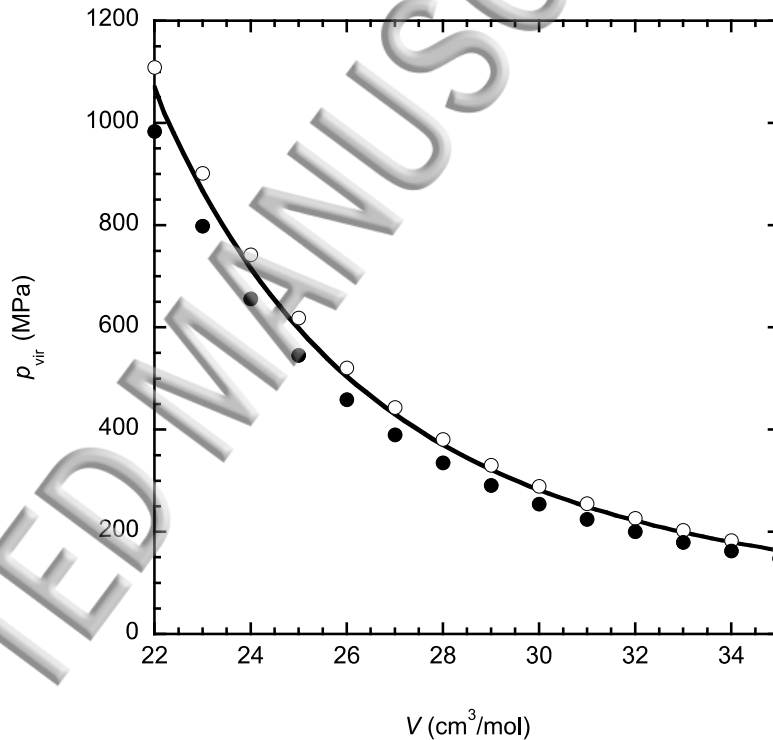
FIG 11. Comparison of the dense fluid p_{vir} behavior of Ar at T = 300 K predicted by the SAAP (●) and the Lennard-Jones potential (○) with experimental data[34] (solid line).

It is apparent from the comparsion of the potential energy obtained form the SAAP illustrated in Fig. 6 that there is a considerable difference with the results obtained for the Lennard-Jones potential at small interatomic separations. Such interatomic separations are commonly encountered at high densities and we would expect the pressures to be considerably affected. Fig. 11 compares the virial

pressure (p_{vir}) by the SAAP and the Lennard-Jones potential for Ar at high densities (small volumes) at the supercritical temperature of 300 K. Slightly lowering the volume of the dense fluid results in a rapid increase in p_{vir}, which quickly approaches and then exceeds 1 GPa. However, it is apparent that p_{vir} obtained from the SAAP is considerably less than the Lennard-Jones values and the difference between the two potentials widens with increasing density. The comparison with experimental data indicates that the excessive repulsion of the Lennard-Jones potential over-predicts the true pressure of dense fluids and solids.

IV. CONCLUSIONS

A new method is reported for developing accurate two-body interatomic potentials, which involves systematically accounting for the salient features of two-body interactions. Using this method, the *ab initio* potential energies of He, Ne, Ar, Kr and Xe can be accurately represented at all separations via a 6 or 7 parameter interatomic potential. The potential avoids the computational complexity of alternative procedures such as the use of the Tang-Toennies formula. Comparison with molecular simulation results indicates that the structures of vapor and liquid phases obtained from the simplified potential are almost indistinguishable from existing more complicated alternatives, providing very good agreement with experimental data. The two-body potential provides a realistic description of repulsion at small interatomic separations and good agreement with experiment for the isochoric heat capacities of Ar at liquid densities.

References

1. C. G. Gray and K. E. Gubbins, *Theory of Molecular Fluids Vol. 1: Fundamentals* (Clarendon Press, Oxford, 1984).

2. G. Marcelli and R. J. Sadus, J. Chem. Phys., **111**, 1533 (1999).

3. M. Vlasiuk and R. J. Sadus, J. Chem. Phys. **146**, 244504 (2017).

4. M. Vlasiuk and R. J. Sadus, J. Chem. Phys. **147**, 024505 (2017).

5. R. J. Sadus, *Molecular Simulation of Fluids: Theory, Algorithms and Object-Orientation* (Elsevier, Amsterdam, 1999).

6. R. Car and M. Parrinello, Phys. Rev. Lett. **55**, 2471 (1985).

7. K. Leonhard and U. K. Deiters, Mol. Phys., **98**, 1603 (2000).

8. A. E. Nasrabad, R. Laghaei and U. K. Deiters, J. Chem. Phys. **121**, 6423 (2004).

9. U. K. Deiters and A. Neumaier, J. Chem. Eng. Data **61**, 2720 (2016).

10. P. S. Vogt, R. Liapine, B. Kirchner, A. J. Dyson, H. Huber, G. Marcelli and R. J. Sadus, Phys. Chem. Chem. Phys., **3**, 1297 (2001).

11. J. A. Barker, R. A. Fischer and R. O. Watts, Mol. Phys. **21**, 657 (1971).

12. R. A. Aziz, J. Chem. Phys. **99**, 4518 (1993).

13. P. Slavíček, R. Kalus, P. Paška, I. Odvárková, P. Hobza and A. Malijevský, J. Chem. Phys. **119**, 2102 (2003).

14. K. Patkowski, G. Murdachaew, C.-M. Fou and K. Szalewicz, Mol. Phys. **103**, 2031 (2005).

15. K. Patkowski and K. Szalewicz, J. Chem. Phys. **133**, 094304 (2010).

16. E. Bich, R. Hellmann and E. Vogel, Mol. Phys. **105**, 3035 (2007).

17. R. Hellmann, E. Bich and E. Vogel, Mol. Phys. **105**, 3013 (2007).

18. E. Bich, R. Hellmann and E. Vogel, Mol. Phys. **106**, 813 (2008).

19. E. Bich, R. Hellmann and E. Vogel, Mol. Phys. **106**, 1107 (2008).

20. R. Hellmann, E. Bich, and E. Vogel, Mol. Phys. **106**, 133 (2008).

21. B. Jäger, R. Hellmann, E. Bich and E. Vogel, Mol. Phys. **107**, 2181 (2009).

22. B. Jäger, R. Hellmann, E. Bich and E. Vogel, Mol. Phys. **18**, 105 (2010).

23. E. Vogel, B. Jäger, R. Hellmann and E. Bich, Mol. Phys. **108**, 3335 (2010).

24. B. Jäger, R. Hellmann, E. Bich and E. Vogel, J. Chem. Phys. **144**, 114304 (2016).

25. B. Jäger, R. Hellmann and E. Bich, J. Chem. Phys. **147**, 034304 (2017).

26. U. K. Deiters, M. Hloucha and K. Leonhard, in *Chemistry for the 21st Century: Chemical Thermodynamics*, edited by T. M. Letcher (Blackwell Science, Oxford, 1999), p. 187.

27. M. Venkatraj, Ch. Bratschi, H. Huber and R. J. Gdanitz, Fluid Phase Equilib. 218, **285** (2004).

28. K. T. Tang and J. P. Toennies, J. Chem. Phys. **80**, 3726 (1984).

29. R. K. Pathak and A. J. Thakkar, J. Chem. Phys. **87**, 2186 (1987).

30. G. Jordan-Engeln and F. Reutter, *Numerische Mathematik für Ingenieure* (Bibliographisches Institut, Mannheim, 1985).

31. J. L. Yarnell, M. J. Katz, R. G. Wenzel and S. H. Koenig, Phys. Rev. A. **7**, 2130 (1973).

32. T. Pfleiderer, I. Waldner, H. Bertagnolli, K. Tödheide, B. Kirchner, H. Huber and H. E. Fischer, J. Chem. Phys. **111**, 2641 (1999).

33. M. Vlasiuk, F. Frascoli and R. J. Sadus, J. Chem. Phys. **145**, 104501 (2016).

34. R. B. Stewart and R. T. Jacobsen, J. Phys. Chem. Ref. Data **18**, 639 (1989).

35. O. Šifner and J. Klomfar, J. Phys. Chem. Ref. Data **23**, 63 (1994).
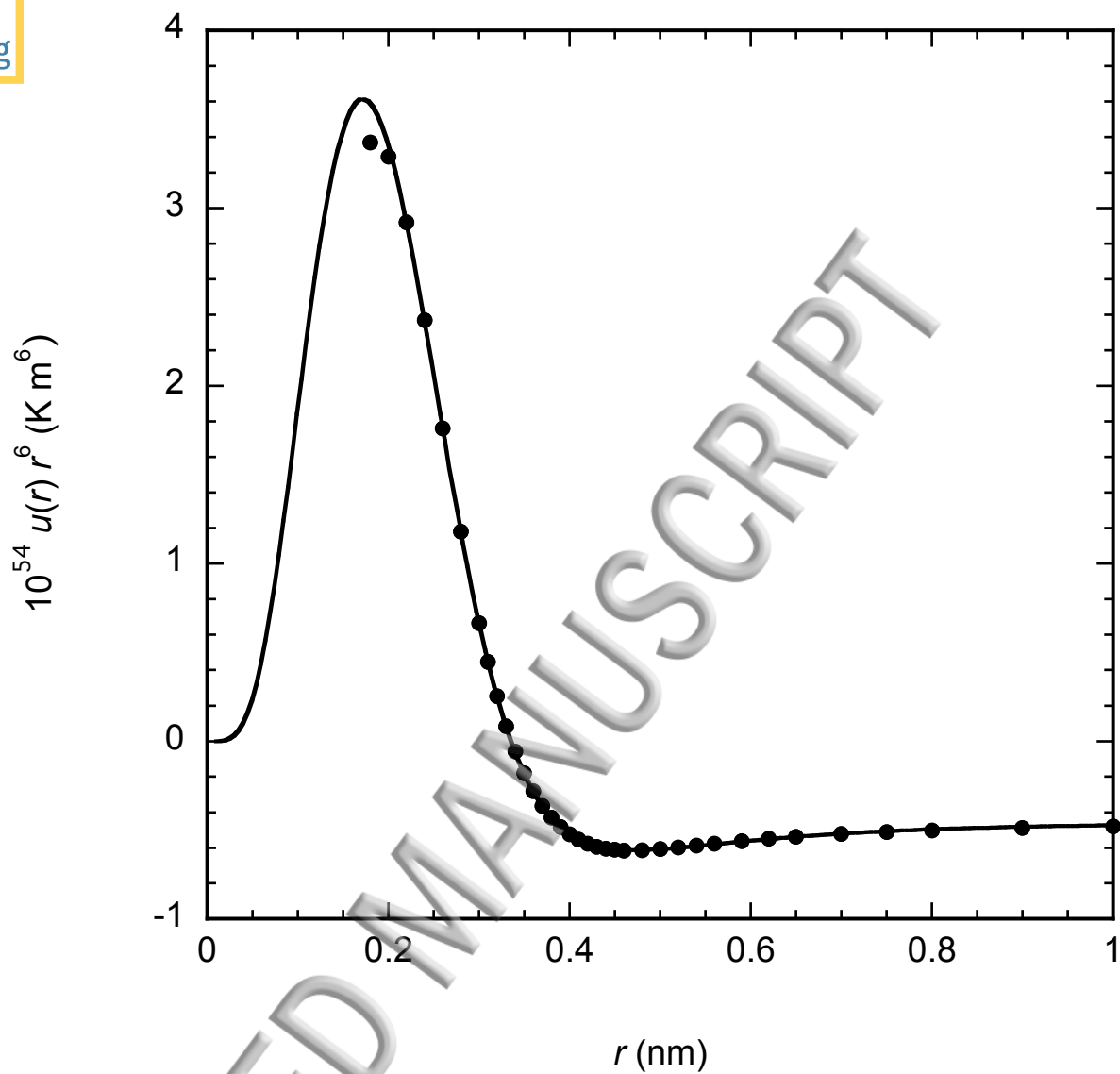
Figure 1
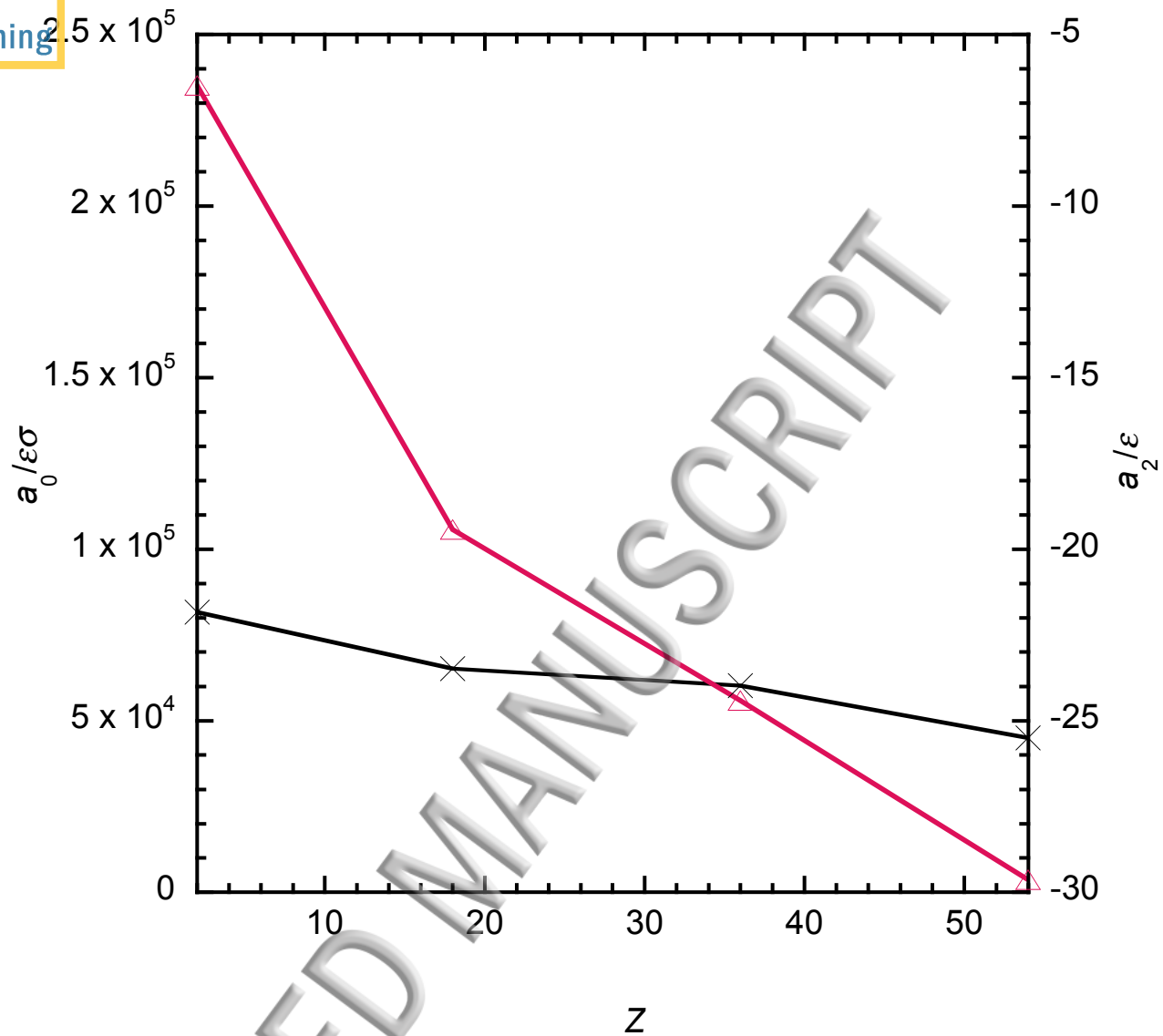
Figure 2
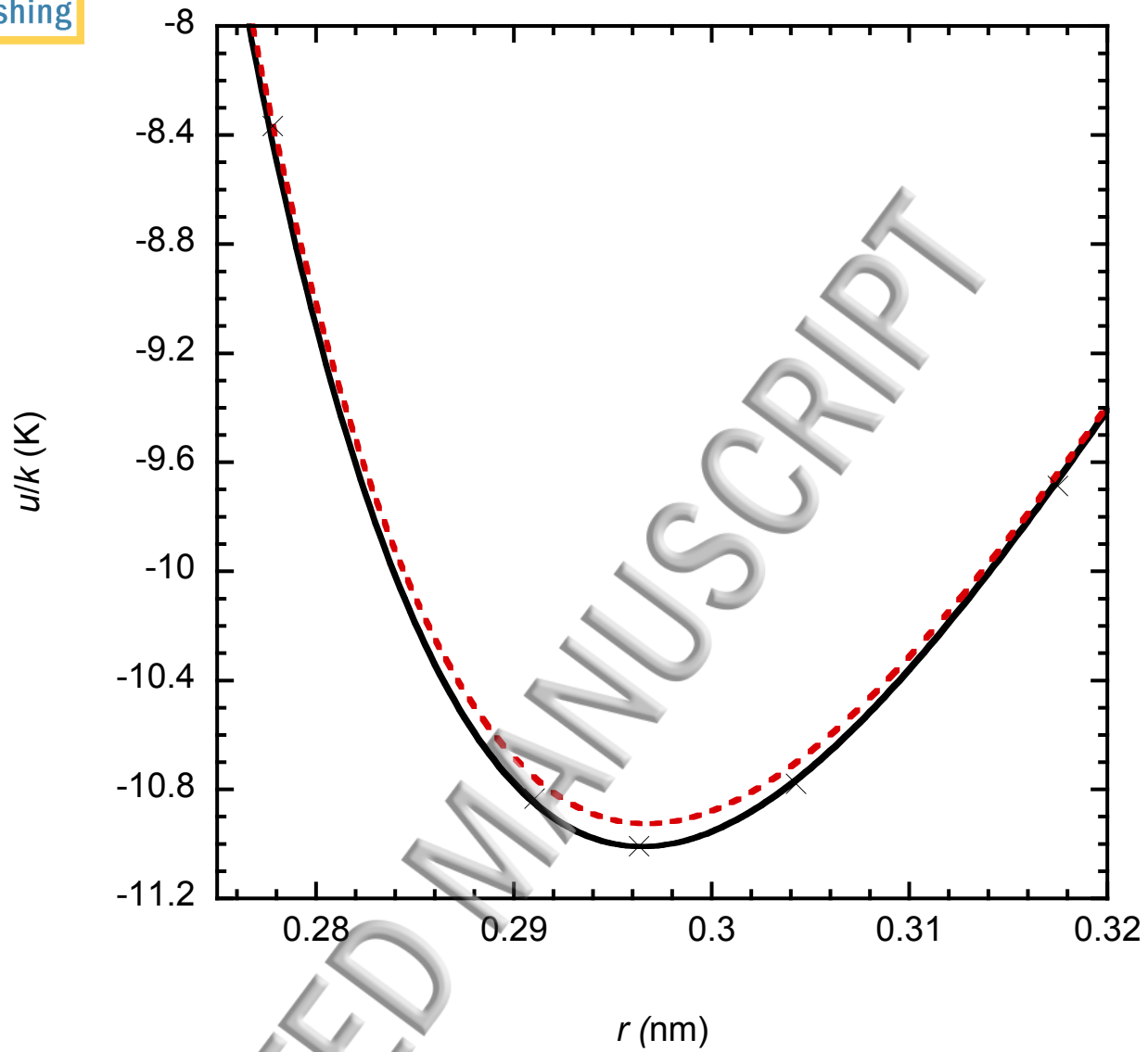
Figure 3
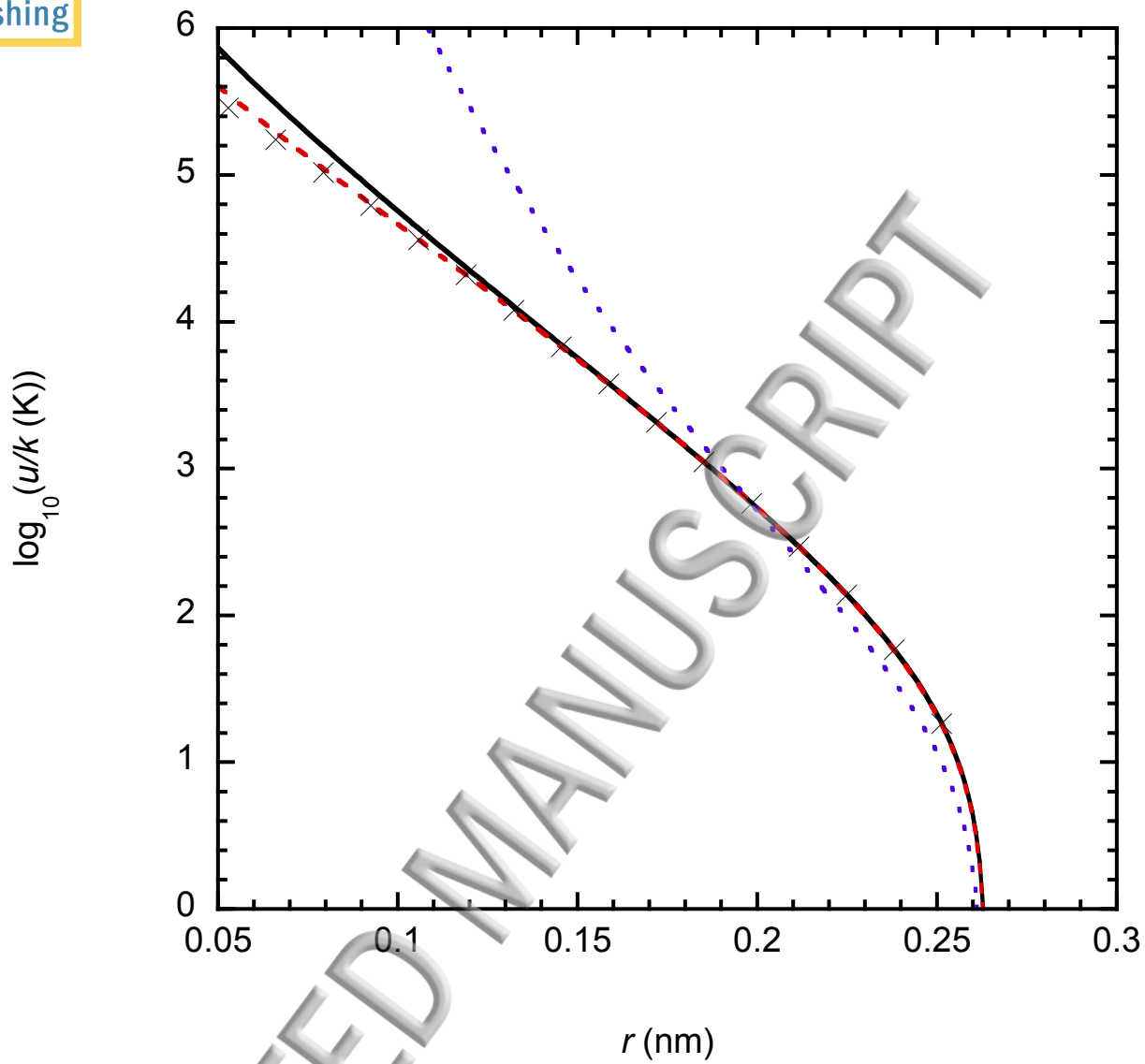
Figure 4
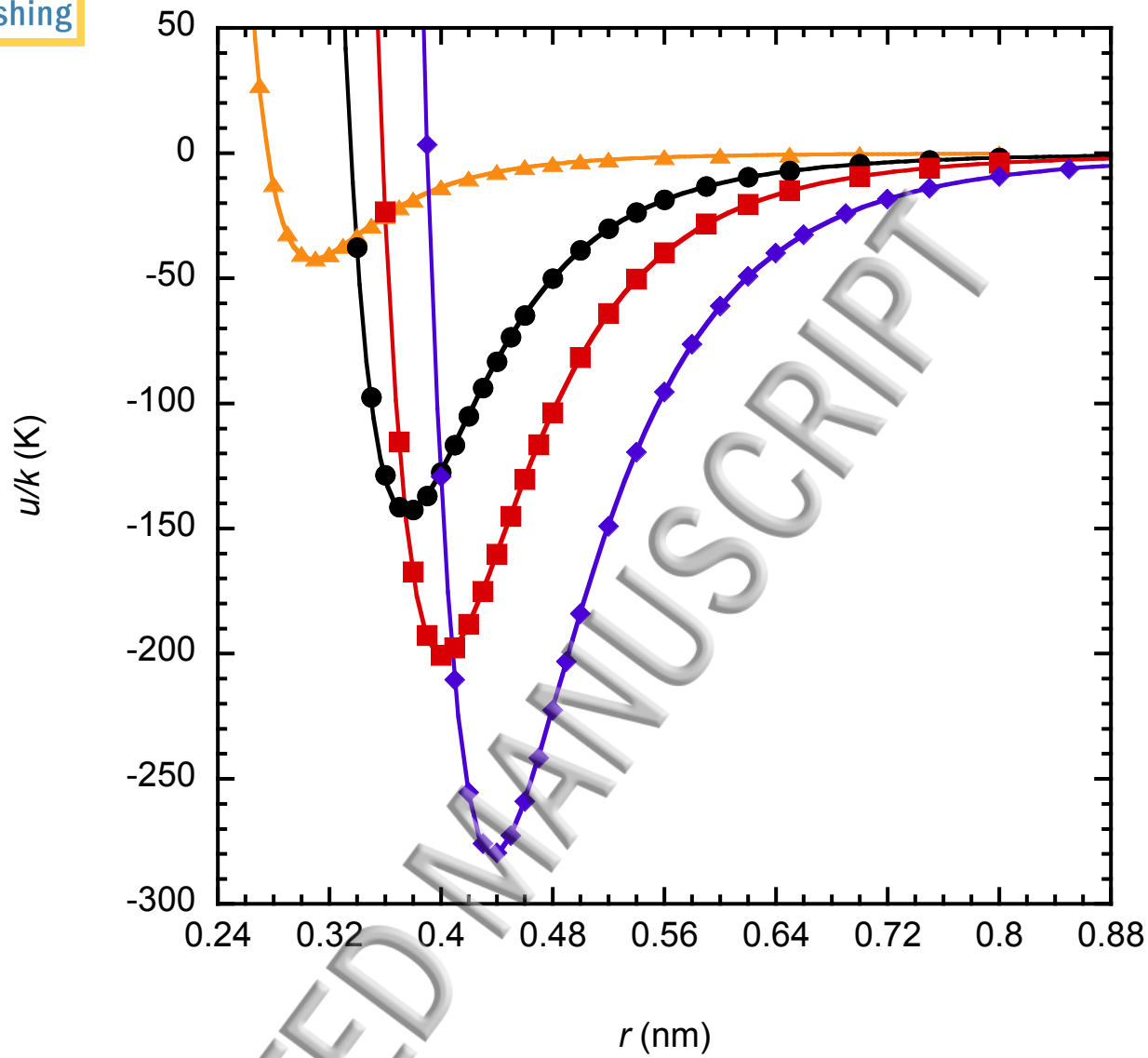
Figure 5
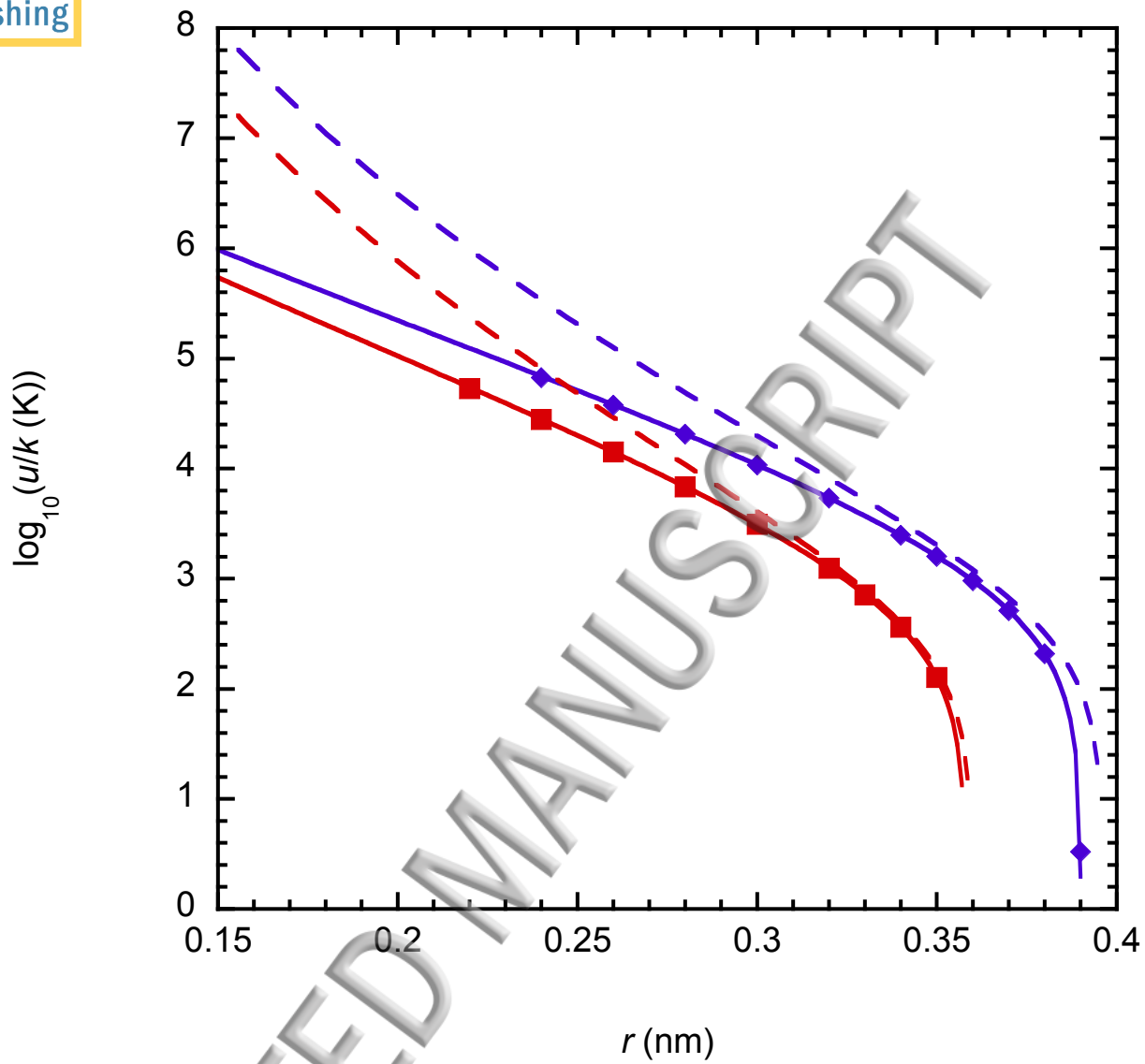
Figure 6
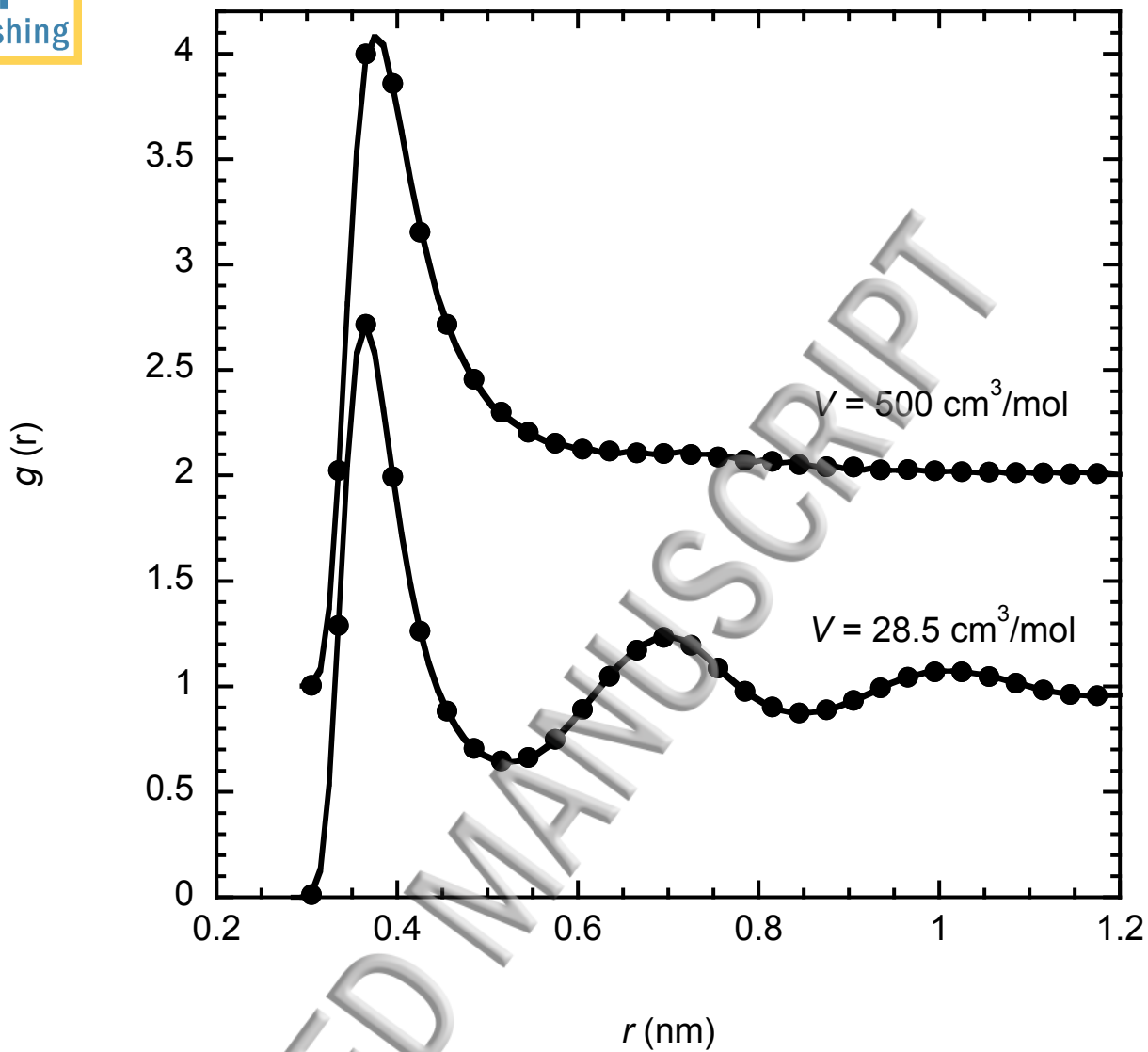
Figure 7
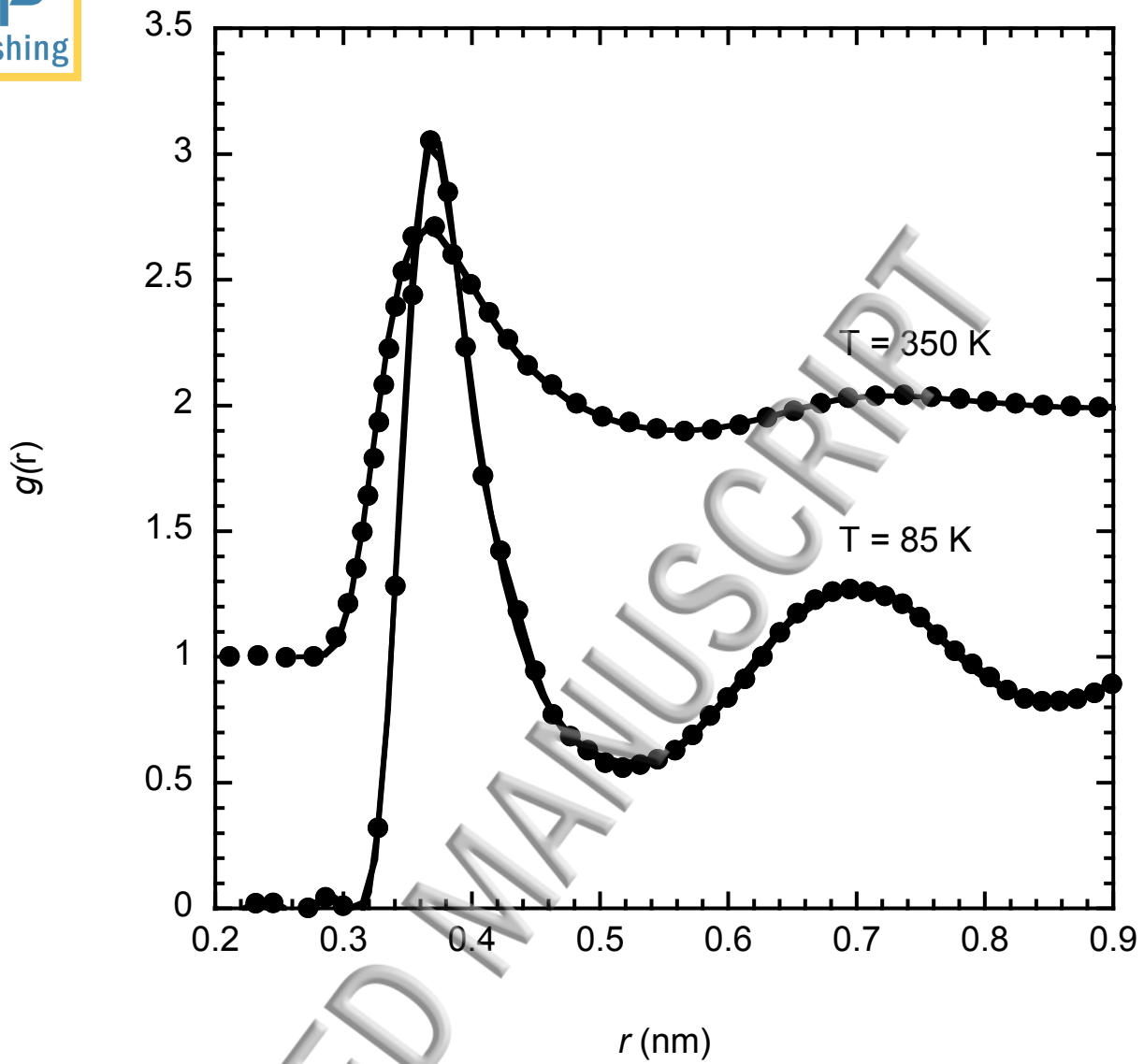
Figure 8
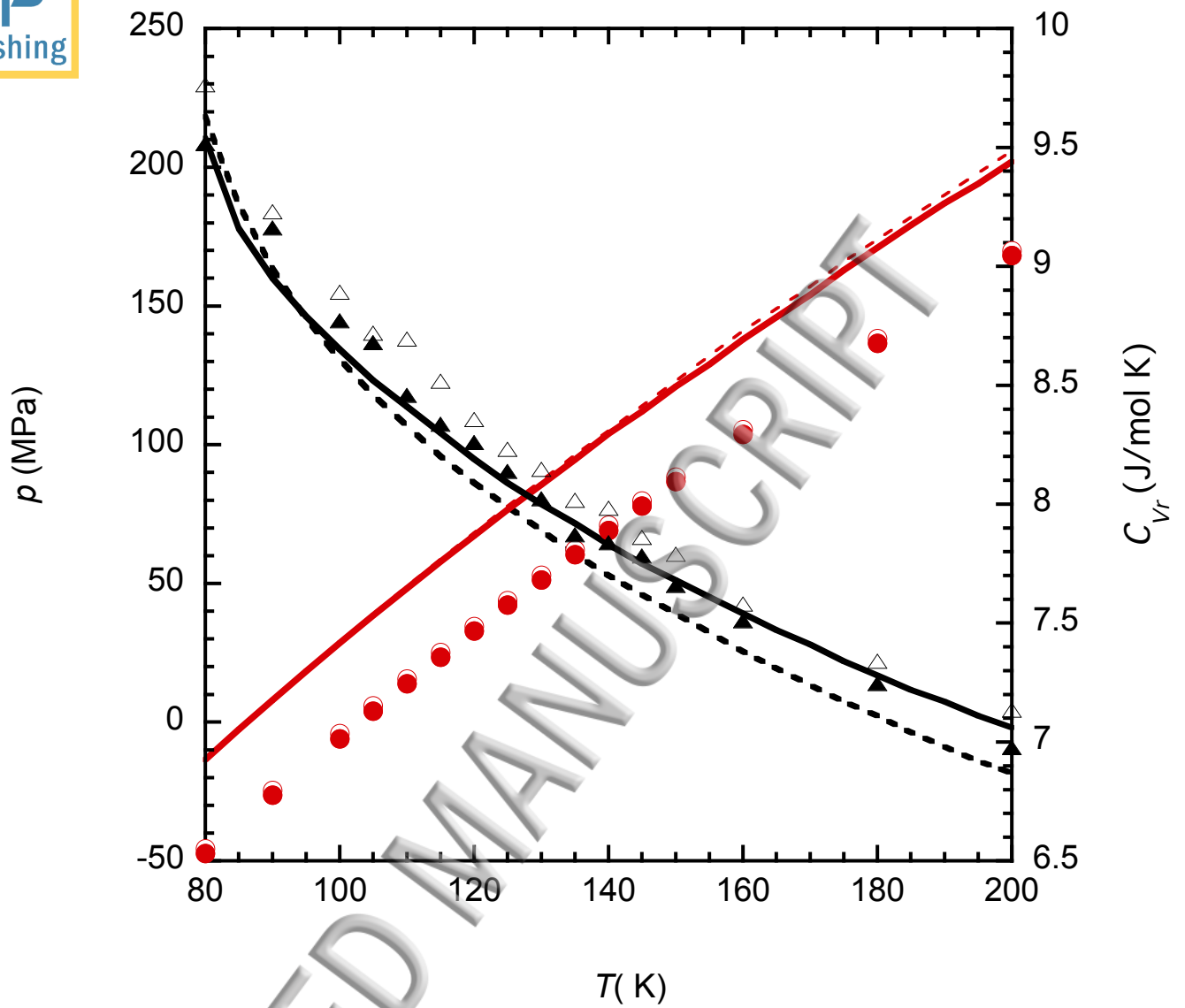
Figure 9

Figure 10

Figure 11